Generation, spectroscopic and chemical characterization of an octahedral iron (V) – nitrido species with a neutral ligand platform

Gerard Sabenya,[a] Laura Lázaro,[a] Ilaria Gamba,[a] Vlad Martin-Diaconescu,[a,*] Erik Andris,[b] Thomas Weyhermüller,[c] Frank Neese,[c*] Jana Roithova,[b,*] Eckhard Bill,[c,*] Julio Lloret-Fillol,*[,d,e] Miquel Costas.*[,a]

a) Institut de Química Computacional i Catàlisi (IQCC) and Departament de Química, Universitat de Girona. Campus Montilivi; E17071 Girona, Catalonia (Spain). miquel.costas@udg.edu, vladmartind@gmail.com

b) Department of Organic Chemistry, Faculty of Science, Charles University in Prague, Hlavova 2030/8, 12843 Prague 2 (Czech Republic). jana.roithova@natur.cuni.cz

c) Max Planck Institut für Chemische Energiekonversion, Stiftstraße 34-36, 45470 Mülheim an der Ruhr (Germany). eckhard.bill@cec.mpg.de, Frank.Neese@cec.mpg.de

d) Institute of Chemical Research of Catalonia (ICIQ), the Barcelona Institute of Science and Technology, Avinguda Paisos Catalans 16, 43007, Tarragona (Catalonia, Spain). jlloret@iciq.es

e) Catalan Institution for Research and Advanced Studies (ICREA), Passeig Lluïs Companys, 23, 08010, Barcelona (Spain).

Abstract

Iron complex $[Fe^{III}(N_3)(MePy_2tacn)](PF_6)_2$ (**1**), containing a neutral triazacyclononane-based pentadentate ligand, and a terminally bound azide ligand has been prepared and spectroscopically and structurally characterized. Structural details, magnetic susceptibility data and Mössbauer spectra demonstrate that **1** has a low-spin (S = 1/2) ferric center. X-Ray diffraction analysis of **1** reveals remarkably short Fe – N (1.859 Å) and long $FeN – N_2$ (1.246 Å) distances, while the FT-IR spectra show an unusually low N – N stretching frequency (2019 cm^{-1}), suggesting that the $FeN – N_2$ bond is particularly weak. Photolysis of **1** at 470 nm or 530 nm caused N_2 elimination and generation of a nitride species that on the basis of Mössbauer, magnetic susceptibility, EPR, and X-ray absorption, in conjunction with DFT computational analyses, is formulated as $[Fe^{V}(N)(MePy_2tacn)]^{2+}$ (**2**). Results indicate that **2** is a low-spin (S =1/2) iron(V) species, which exhibits a short Fe-N distance (1.64 Å), as deduced from EXAFS analysis. Compound **2** is only stable at cryogenic (liquid N_2) temperatures, and frozen solutions as well as solid samples decompose rapidly upon warming, producing N_2. However, the high-valent compound could be generated in the gas phase and its reactivity against olefins, sulphides and substrates with weak C-H bonds studied. Compound **2** proved to be a powerful two-electron oxidant that can add the nitride ligand to olefin and sulphide sites, as well as oxidize cyclohexadiene substrates to benzene in a formal H_2 transfer process. In summary compound **2** constitutes the first case of an octahedral $Fe^{V}(N)$ species prepared within a neutral ligand framework, and adds to the few examples of Fe^{V} species that could be spectroscopically and chemically characterized.

Introduction

High-valent iron compounds are highly reactive species that are involved in a number of reactions of interest in biology, chemical synthesis and technology.[1-7] For instance high-valent iron-oxo species are key intermediates in challenging oxidation reactions such as C-H hydroxylation[8-10] and water oxidation,[11-13] while high-valent nitride and related species have been considered as possible intermediates in iron-mediated dinitrogen reduction to ammonia. One of the mechanisms proposed for the latter process is the release of ammonia and the generation of a high valent $Fe^{IV}\equiv N$ intermediate, which in biology is suggested to take place at a single iron site on the FeMo cofactor of nitrogenase.[14]

The nitride ligand is regarded as particularly suitable for stabilizing such high oxidation states because of its negative charge, and its powerful σ and π donor abilities. Nevertheless, preparation and characterization of octahedral high-valent iron species with terminal nitride ligands in non porphyrinic environments remains a challenge for synthetic inorganic chemistry, although their reactivity is of high interest.[4,15-19] In contrast, quasi-tetrahedral iron(IV) – nitride species can be made relatively stable by using bulky ligands and their reactivity was explored in some detail.[20-26] Nitride transfer to styrene,[26] isocianides[24] and triarylphosphines[27] has been documented. In addition, reaction with cyclohexadienes has been shown to proceed *via* cycloaddition and hydrogen-abstraction.[25] Peters and Smith have independently shown that bimolecular reactions between iron(IV) – nitride complexes lead to Fe^{I}-NN- Fe^{I} dimeric species.[20,21] Some of these complexes also reacted with water protons and electrons to afford quantitative amounts of ammonia.[28]

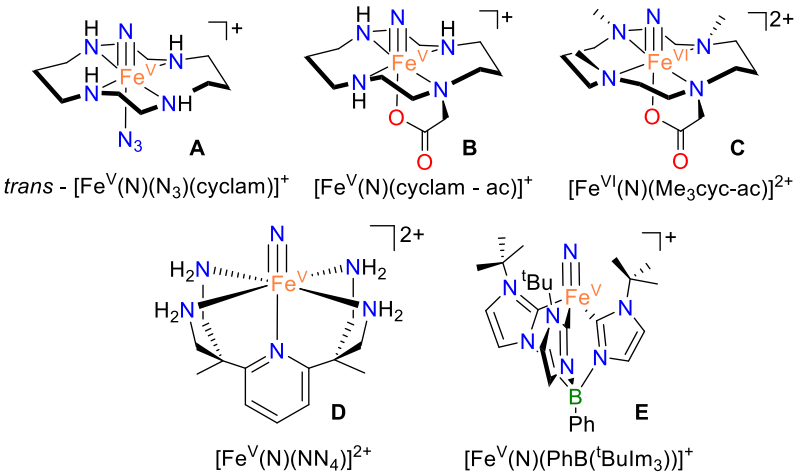

Scheme 1. Representative examples of non-heme iron(V) nitride complexes within the cyclam (**B**),[29](**A**)[30] and tetrapodal pentadentate (NN_4, **D**)[31] tetragonal frameworks as well as pseudo-tetrahedral iron(V) nitride (**E**)[32] and iron(VI) nitride species (**C**)[33] reported in the literature.

Nitridoiron(V) porphyrins were first described by Nakamoto *et al*, produced by laser irradiation of thin films of the corresponding azido complexes at -30 K, but could only be characterized by resonance Raman.[19] Pioneering examples of iron(V) nitrido species in octahedral environments were described by Wieghardt *et al*, via photolysis of the corresponding ferric – azide precursors in frozen matrices.[29,30] The same authors also described preparation of an iron(VI) nitrido species by photolysis of the corresponding iron(IV) – azide complex.[33] The use of the frozen matrix proved crucial for the successful preparation of these species. However, attempts to prepare analogous complexes with anionic triazacyclononane based pentadentate ligands resulted instead in the generation of ferrous complexes via homolytic cleavage of the Fe – N_{azide} bond.[34] Most remarkably, Smith and Meyer have recently described the preparation and structural characterization of an iron(V) – nitride species with a sterically encumbered tris – carbene ligand that enforces a distorted tetrahedral geometry.[32,35]

With the single exception of the latter, iron(V) – nitride species can only be prepared in frozen solutions at cryogenic temperatures, and their reactivity remains poorly explored. The iron(V) – nitride species described by Smith and Meyer has been shown to react with water to produce ammonia,[32] while N – N coupling has been documented in the thermal decomposition of $[Fe^{V}(N)(cyclam - ac)]^{+}$ and *trans* – $[Fe^{V}(N_3)(N)(cyclam)]^{+}$.[36] Furthermore, formation of *trans* – $[Fe^{V}(N_3)(N)(cyclam)]^{+}$ by N_2 extrusion from the ferric – azide precursor, and its reaction with triphenylphosphine has been monitored by real time FT-IR.[37] Gas phase reactivity has also proven to be a convenient tool to generate and study the chemistry of highly reactive high valent iron-nitride species,[31,38] although ligand degradation appears to be a competing or even a dominating path in some of the previous studies.[38]

Overall, these precedents evidence that examples of high-valent iron – nitride species remain scarce. Their high reactivity makes them very interesting but at the same time hampers their preparation and the study of their reactivity. With these considerations in mind, we targeted the synthesis, and characterization of a novel octahedral iron(V) – nitride species, and the investigation of its reactivity. Towards this end, this work describes the photolysis of the iron – azide complex $[Fe^{III}(N_3)(MePy_2tacn)](PF_6)_2$ (**1**, $MePy_2tacn$ = N – methyl – N, N – bis(2– picolyl) – 1, 4, 7 – triazacyclononane) to generate the corresponding high-valent iron(V) species $[Fe^{V}(N)(MePy_2tacn)]^{2+}$ (**2**), which has been spectroscopically characterized by a combination of methods (Mössbauer, magnetic susceptibility, EPR, and X – ray absorption spectroscopy) as well as DFT computational analysis. While previously described octahedral iron(V)-nitride complexes have aliphatic polyamine ligands (scheme 1), **2** bears an oxidatively more robust polypyridyl ligand scaffold. This element endorses **2** with a comparatively enhanced stability which permits its generation in nearly quantitative yields. Complex **2** is only stable at very low temperatures in frozen solution but its reactivity against external substrates can be studied in the gas phase.

Therefore, **2** constitutes a very rare example of an iron(V) species that could be spectroscopically characterized and whose reactivity could be explored.

Results and Discussion

Synthesis and characterization of $[Fe^{III}(N_3)(MePy_2tacn)](PF_6)_2$ (1).

Ferric species $[Fe^{III}(N_3)(MePy_2tacn)](PF_6)_2$ (**1**), was prepared by reacting equimolar amounts of iron(III) triflate and the $MePy_2tacn$ ligand in THF under anaerobic conditions (Figure 1, left) . The resulting reddish solution was evaporated under vacuum, and the resulting solid was dried and solved in water followed by addition of excess NaN_3. The solution was stirred for ~2 hours and a saturated solution of $NaPF_6$ or NH_4PF_6 was added with continuous stirring for an additional ~2 hours. A purplish solid precipitate was formed, filtered and recrystallized in acetone using diethyl ether diffusion. The final product is a ^1H – NMR silent ferric – azide species $[Fe^{III}(N_3)(MePy_2tacn)](PF_6)_2$ (**1**) as characterised by Mössbauer, UV – vis, IR, Raman, EPR, magnetic susceptibility and mass spectrometry.

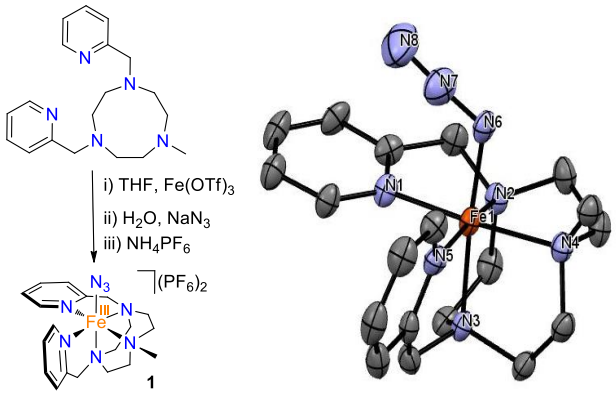

Figure 1. (Left) Schematic diagram for the preparation of complex **1**. (Right) Solid-state structure of **1** with ellipsoids set at 50% probability. Protons and hexafluorophosphate $(PF_6)^-$ anions were omitted for clarity. Selected bond distances and angles: Fe(1) – N(6), 1.859(5) Å; N(6) – N(7), 1.246(7) Å; Fe(1) – N(6)-N(7), 122.2(4)º.

The solid-state structure of **1** could be determined by single crystal X – ray diffraction analysis. Figure 1 (right) shows the ORTEP diagram of the cationic part of the complex with selected bond lengths and angles. The complex contains an iron center in a distorted octahedral coordination geometry having five coordination sites occupied by the N atoms of the neutral ligand framework and one azide anion to complete the coordination environment. One of the coordinating pyridines is coplanar to the Fe – N_3 axis, while the second is perpendicular to this axis. Furthermore, the azide and the pyridine ligands are *trans* to N atoms of the tacn moiety. Interestingly, in **1** the Fe – N(6) bond is remarkably shorter at 1.859 Å and the FeN(6) – N(7) bond remarkably longer at 1.246 Å, than in any of the previously described ferric – azide

complexes (Table 1). Literature precedents show that low-spin (S = 1/2) ferric complexes exhibit shorter Fe – N and larger FeN – N_2 distances than high-spin ferric complexes, but the values measured for **1** presumably also reflect a higher electrophilicity of the ferric center due to the neutral character of the $MePy_2tacn$ ligand. Instead, previous examples of ferric – azide complexes (Table 1) contain anionic ligands that compensate the positive charge of the ferric center.

The zero-field Mössbauer spectrum of **1** recorded at 80 K shows a single doublet with low isomer shift and large quadrupole splitting, δ = 0.21 mm·s^{-1}, ΔE_Q = 2.13 mm·s^{-1} (Figure 2-top). These values are characteristic of low-spin iron(III) centers which is in agreement with the effective magnetic moments of 1.5 - 1.8 μ_B measured between 10 and 300 K (Figure S2). Consistently, the EPR spectrum of **1** in frozen acetone solution at 10 K is also characteristic of a low-spin iron(III) (S = 1/2), showing rhombic symmetry with simulated g values g_1 = 2.58, g_2 = 2.26 and g_3 = 1.83 (Figure 2-bottom).

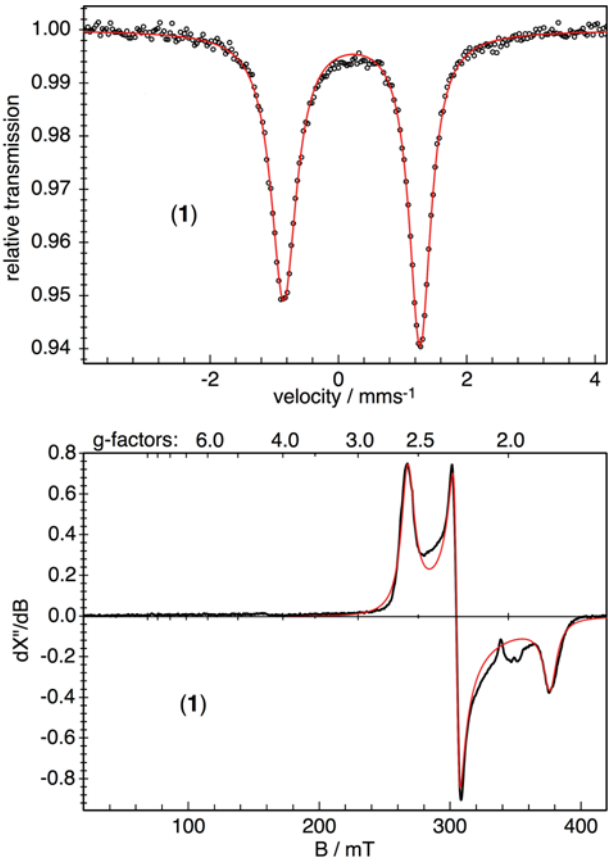

Figure 2. (top) Zero-field Mössbauer spectrum of solid **1** at 80 K, and (bottom) X-band EPR spectra of **2** in frozen acetone solution at 10 K (frequency 9.6437 GHz, power 0.2 mW, modulation 0.75 mT / 100 kHz). The EPR derivative amplitudes are given in arbitrary units. The red lines in both spectra are simulations. The asymmetry of the Mössbauer spectrum results from a difference in line widths, presumably due to intermediate spin relaxation of the half-integer spin system, or/and due to slight heterogeneity of iron sites in the powder sample.

The resonance Raman spectrum of complex **1** exhibits a weak signal at 2026 cm^{-1}, assigned to the asymmetric stretching of the coordinated azide, whereas the FT – IR spectra shows a single peak at 2019 cm^{-1}, assigned to the azide stretching vibration (Figure S1).[39] Moreover, when **1** was prepared using ^{15}N terminally labelled sodium azide, its IR spectrum exhibited two features at 2021 and 1998 cm^{-1} equal in intensity, assigned to the N – N stretching mode. The ν(N – N) downshift from 2021 cm^{-1} to 1998 cm^{-1} ($\Delta\nu$ = 23 cm^{-1}) is lower than the expected 33 cm^{-1} shift for a diatomic N – N oscillator. This suggests that the observed features are not only reflecting the stretching from the N – N bond but possibly a contribution of the rest of the azide moiety or of the iron centre to the observed vibrations.

Of particular interest is also the lower frequency of the N – N stretching frequency of **1** when compared with the other ferric – azide complexes described in Table 1. The energy of stretching vibrations observed by FT-IR spectroscopy nicely agree with the metrical parameters of the Fe – N_{azide} unit determined from the crystallographic structure of **1**, and conversely indicate that the Fe – N bond is particularly strong while the FeN-N bond is unusually weak. The structural and spectroscopic data therefore suggest that the FeN-N bond could be readily activated towards breakage and release of N_2.

Table 1. Azide stretching frequencies and Mössbauer parameters for the studied (top) and bibliography compounds (below).

Compound	ν (cm^{-1})	Spin State	Fe – N distance (Å)	FeN – N distance (Å)	δ ($mm \cdot s^{-1}$)	ΔE_Q ($mm \cdot s^{-1}$)
NaN_3	2120	---	---	---	---	---
$[Fe^{III}(N_3)(MePy_2tacn)](PF_6)_2$ (1)	2019	S = 1/2	1.859	1.246	0.21	2.13
$[Fe^{III}(^{15}NN_2)(MePy_2tacn)](PF_6)_2$	2021 1998	ND	ND	ND	ND	ND
[b] $[Fe^{III}(N_3)$(cyclam – ac)$](PF_6)$	2051	S = 1/2	1.931	1.209	0.27	2.53
[c] *cis* - $[Fe^{III}(N_3)_2$(cyclam)$](ClO_4)$	2078 2047	S = 5/2	1.976 1.970	1.194 1.210	0.46	0.29
[c] *trans* - $[Fe^{III}(N_3)_2$(cyclam)$](ClO_4)$	2044	S = 1/2	1.937	1.180	0.29	2.26
[d] $[Fe^{III}(N_3)(Ac_2tacnCH_2C_6H_4OMe)]$	2064	S = 5/2	---	---	0.56	0.47
[d] $[Fe^{III}(N_3)(Ac_2tacn^iPr)]$	2066	S = 5/2	1.981	---	0.46	0.82
[d] $[Fe^{III}(N_3)(Ac_2tacnCH_2C_6H_5)]$	2066	S = 5/2	1.975	---	0.46	0.61
[c] *trans* - $[Fe^{II}(N_3)_2$(cyclam)$](ClO_4)$	---	S = 0	---	---	0.55	0.72
[c] *cis* - $[Fe^{II}(N_3)_2$(cyclam)$](ClO_4)$	---	S = 2	---	---	1.11	2.84

ND: Not determined. [a] Component from the mixture that was attributed to $Fe^{III}(N_3)$. [b] ref [29]. [c] ref [30]. [d] ref [34].

Complex **1** was also analysed by mass spectrometry (Figure S4). The spectrum shows a major peak at m/z = 211.58 with an isotopic pattern indicative of an $[Fe^{III}(N_3)(MePy_2tacn)]^{2+}$ ion. Interestingly, the spectra showed two additional peaks at m/z = 190.58 and 197.58 that can be assigned to $[Fe^{II}(MePy_2tacn)]^{2+}$ and $[Fe^{V}(N)(MePy_2tacn)]^{2+}$ ions, respectively. Tandem mass spectrometry/mass spectrometry (MS/MS) analysis shows that they both proceed from fragmentation of the m/z = 211.58 ion, indicating they originate from the cleavage of the Fe – N and the N – N bonds of the azide complex, respectively. High resolution mass spectrometry of ^{15}N labelled complex $[Fe^{III}(^{15}N_3)(MePy_2tacn)](PF_6)_2$ (**1 – ^{15}N**) (Figure S5) confirmed the assignment of the ions observed in **1**. As the azide anion is labelled in one of the two terminal positions, both the $[Fe^{V}(^{14}N)(MePy_2tacn)]^{2+}$ and $[Fe^{V}(^{15}N)(MePy_2tacn)]^{2+}$ were observed in a 1:1 ratio, where each of these ions (m/z = 197.58 and 198.08), are formed from N – N cleavage on the $[Fe^{III}(N_2{=}^{15}N)(MePy_2tacn)]^{2+}$ and $[Fe^{III}(^{15}N{=}N_2)(MePy_2tacn)]^{2+}$ respectively. These observations, again, evidence the possibility to cleave the N – N bond to gain access to high – valent iron species.

Photolysis of $[Fe^{III}(N_3)(MePy_2tacn)](PF_6)_2$ (1).

Photolysis in solution. When acetonitrile solutions of **1** were photolysed at 233 K with blue or green LED lamps (470 or 530 nm, respectively) for a few minutes (15 – 20 min), formation of $[Fe^{II}(CH_3CN)(MePy_2tacn)]^{2+}$ (**3**) occurs, as revealed by UV-Vis spectroscopy.[40] Monitoring the reactions by UV-Vis revealed that the process occurs with isosbestic points, thus reflecting a clean transformation presumably entailing formation of azide radicals via homolytic cleavage of the Fe-N bond without significant accumulation of other species (reduction of **1** with 470 nm irradiation is shown in Figure S6). Such behaviour has previously been reported for analogous iron(III) complexes with cyclam ligands[29,30] and led us to further explore the reactivity in solid samples and frozen solutions at cryogenic temperatures to investigate the formation of possible high-valent iron intermediates

Photolysis of solid powder samples. Solid powder samples of **1** were finely dispersed in an open liquid nitrogen bath and photolysed under stirring at 77 K for ~5 h. Upon irradiation with 470 nm light, zero-field Mössbauer reveals consumption of the initial iron(III) – azide complex **1,** and generation of two new species attributable to 26 % of low-spin iron(II) (δ = 0.38 mm·s^{-1}, ΔE_Q = 0.67 mm·s^{-1}) and 74 % of a new component (**2**). This latter subspectrum is broad and asymmetric, as expected for half-integer spin with intermediate spin relaxation. An approximate fit with an asymmetric quadrupole doublet revealed a remarkably low isomer shift (δ) of approximately -0.01 mm·s^{-1} and moderately large quadrupole splitting (ΔE_Q) of *ca.* 1.02 mm·s^{-1} consistent with the formation of a high-valent iron center (Figure S8-A). Magnetic susceptibility experiments of the ferric starting complex **1** after photolysis (see Figure S9) also show a sample

composition of 25 % of iron(II) with S = 0, and 75 % of complex **2** with S = ½, having an effective magnetic moment that varied from *ca.* 0.9 μ_B at 2 K to *ca.* 1.4 μ_B at temperatures above 10 K. Irradiation with 530 nm light also yielded quantitative conversion of the ferric starting material, with only *ca.* 5 % of initial iron(III) left over in the Mössbauer spectrum (and 14 % of an initial ferrous impurity that did not change during irradiation; Figure S8-B). However, only 4% of the low-spin iron(II) photo-product was detected (δ = 0.39 mm·s^{-1}, ΔE_Q = 0.70 mm·s^{-1}, previously 25%), and 78 % of the high-valent iron (**2**) subspectrum (δ = 0.0 mm·s^{-1}, ΔE_Q = 0.86 mm·s^{-1}). In summary, this reveals 95 % conversion of the ferric **1** azide compound into the high-valent compound **2** using 530 nm light, in contrast to 75% achieved by photolysis at 470 nm. Therefore generation of **2** in frozen solution samples was further investigated using irradiation with 530 nm light.

Photolysis of frozen solution samples with 530 nm light. Additional preparations with 530 nm light using 2 mM frozen (~77 K) acetone solution samples of **1** were investigated. After ~5 hours irradiation the solution changed color from purple to orange. Follow up Mössbauer analysis (Figure 3, top panel) revealed virtually complete conversion of **1** into **2** (δ = -0.01 mm·s^{-1}, ΔE_Q = 1.09 mm·s^{-1}). By comparison with the iron(V) complexes $[Fe^V(N)(N_3)(cyclam)]^+$ and $[Fe^V(N)(cyclam\text{-}ac)]^+$ (δ = -0.04 and -0.01 mm·s^{-1}, ΔE_Q = 1.90 and 1.58 mm·s^{-1}, respectively),[29,30,36] the Mössbauer spectrum of the photoproduct (**2**) can be assigned, in particular due to its low isomer shift, to a high-valent nitrido iron(V) complex with spin S = 1/2. This conclusion could be supported by an EPR analysis of **1** photolysed in frozen solution inside a sealed EPR tube under vacuum (Figure 3, lower panel). The EPR spectra recorded before and after irradiation show quantitative consumption of the starting material (**1**) and formation of a new EPR signal at remarkably low g ≈ 1.27. That derivative signal can be assigned to the $g_\perp$ resonances of a slightly rhombic spectrum for which a simulation yielded g-values of 1.59, 1,33, and 0.9 (inset of Figure 3 lower panel, red line). Numerical double integration of that spectrum, which we assign to **2**, and comparison with the starting material, reveals *ca.* 50% recovery of the spin concentration after photolysis (after division with the appropriate Aasa-Vanngard[41] factors of 2.24 for the spectrum of **1** and 1.27 for the spectrum of **2** to account for different g values, 20-30% error possible). The unusually low g values of **2** which deviate significantly from the typical g splitting around g=2 as encountered for low-spin ferric compounds like **1,** render **2** experimentally a nitrido iron(V) complex with S = ½ and substantially unquenched orbital moment, apparently due to orbital degeneracy in the corresponding low-spin $3d(t_{2g})^3$ configuration. To the best of our knowledge, EPR data from iron(V) – nitride compounds are reported only for the pseudo tetrahedral complex $[Fe^V(N)(^tBuIm_3BPh)]^+$ (S = 1/2, $g_\perp$ = 1.971, $g_{//}$ = 2.299),[32] and for the octahedral complexes $[Fe^V(N)(cyclam\text{-}ac)]^+$ (g_1 = 1.629 and g_2 = 1.746, g_3 = 1.036,) and

$[Fe^{V}(N)(N_3)(cyclam)]^{+}$ ($g_1 = 1.626$, $g_2 = 1.748$, $g_3 = 0.985$).[42] Apparently the ligand-field situation of **2** resembles that of the quasi octahedral, cyclam-based nitrido iron(V) species and its observed EPR resonances fall within the same range of $g_{\perp}$ values.

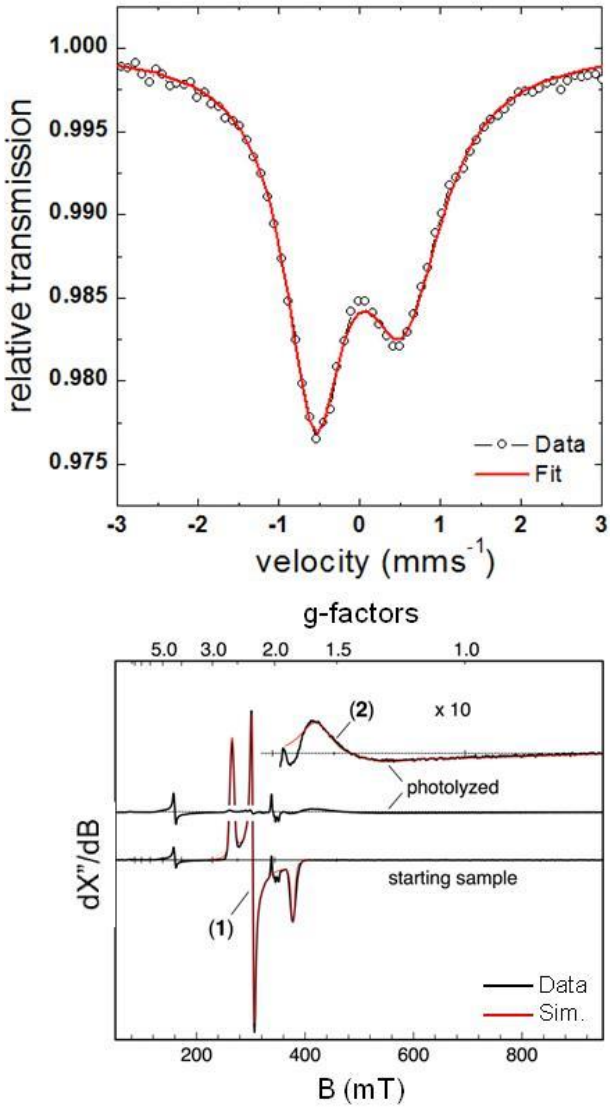

Figure 3. (top) Zero-field Mössbauer spectrum of a 2 mM frozen solution of complex **1** enriched with ^{57}Fe after 5 h photolysis at 77 K with a 530 nm (green) LED fitted with a Lorentzian doublet accounting for the high-valent photo-product **2** (~100%, red line); (bottom) EPR spectrum of a 2 mM frozen solution sample from the same batch in a sealed EPR tube under vacuum recorded before and after photolysis (T = 10 K, frequency 9.6468 GHz, power 0.5 mW, modulation 0.75 mT / 100 kHz).The red line shown in the inset is a simulation for the photo-product with g values $g_1 = 1.59$, $g_2 = 1.33$ and $g_3 = 0.9$.

X-Ray Spectroscopy

The series of complexes **1**, **2** and $[Fe^{II}(N_3)(MePy_2tacn)]^{2+}$ (**4**) (details of its preparation and characterization can be found in the supporting information) was also characterised by Fe K-edge X-ray absorption spectroscopy (XAS), providing further insight into the electronic and geometric structure of **1** and **2** (Table 2, Figure 4 and Figure S10). The rising edge spectra (Figure 4 – left) for **4**, **1** and **2** are consistent with a sequential increase in the metal oxidation state. Compound **4** with a rising edge energy of 7120.6 eV, has a small pre-edge feature attributed to 1s→3d dipole forbidden transitions at ~7111.6 eV with an intensity of ~0.045 normalized units. This is consistent with a low-spin octahedral iron(II) centre having dipole forbidden pre-edge transitions to the e_g set of orbitals.[43] Compound **1** on the other hand experiences a shift in its rising edge to 7122.7 eV concomitant with a 1 eV shift in its pre-edge intensity weighted average energy. The pre-edge of **1** can be fit with two low intensity peaks at 7111.9 eV and 7113.2 eV similar to previously reported low-spin hexacoordinate iron(III) complexes. Lastly, **2** was generated by irradiating a 4 mM frozen solution of **1** in acetone for 5 h at 77 K during which the colour progressively changed from purple to orange (*vide supra*). Compound **2** has a rising edge at 7123.8 eV with a very intense pre-edge at 7114.2 eV and a shoulder at 7112.4 eV giving an intensity weighted average pre-edge of 7113.9 eV. Such a profile correlates with the previously reported values for the XAS spectra of the related $[Fe^{V}(N)(cyclam-ac)]^{+}$ complex having a rising edge of ~7124.1 eV and a pre-edge energy of 7113.9eV.[44,45] Furthermore the pre-edge energy of **2** is below that of $[Fe^{VI}(N)(Me_3cyclam-ac)]^{+}$ (7114.4 eV) strongly pointing to the formation of an iron(V) center.[33,44,45] To obtain insight into the coordination structure of **2**, EXAFS analysis was carried out. A picture emerges of a six-coordinate metal center consisting of N/O scattering atoms having a short 1.64 Å Fe-N/O bond. Presumably this corresponds to the short Fe – nitride bond that causes a tetragonal distortion of the octahedral geometry and facilitates p-d mixing through a strong metal – ligand covalent interaction resulting in a very intense pre-edge.[44] Previous researchers have reported similar Fe – nitride bond lengths of 1.61 Å for the $[Fe^{V}(N)(cyclam-ac)]^{+}$ complex and 1.57 Å for $[Fe^{VI}(N)(Me_3cyclam-ac)]^{+}$.[33,44] Comparing these values to the related $[Fe^{V}(N)(^{t}BuIm_3BPh)]^{+}$ complex, with an Fe – N bond of 1.502(2) Å, we have a sensibly longer bond. This can be rationalised by the fact that **2** is a hexacoordinate complex and the former is a tetradentate complex in pseudo – tetrahedral geometry, which translates to a shorter Fe – N bond for a lower coordination number.[32]

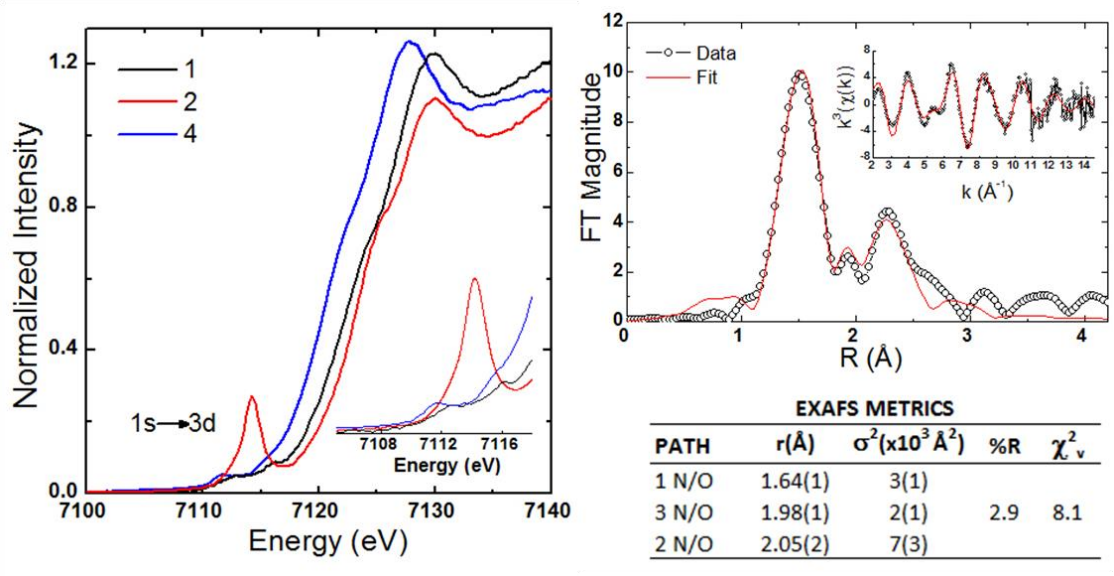

Figure 4. (Left) Iron K – edge X – ray absorption spectra of **1** (black), **2** (red) and **4** (blue). The inset is an expansion of the pre – edge region. (Right) Fourier transformed EXAFS spectra of **2** (inset:. k^3-weighted unfiltered EXAFS spectra (Data: black circles; Fits: red line).

Table 2. Comparison of Fe – N bond distances and XAS energies.

Complex	Fe - N distances (DFT) (Å)	XAS Energies		1s→3d Pre-edge Intensities
		E^o (eV)	$E_{pre\text{-}edge}$ (eV)	
$Fe^{II}(N_3)(MePy_2tacn)](PF_6)$	(2.02)	7120.6	7111.6	0.045
$[Fe^{III}(N_3)(MePy_2tacn)](PF_6)_2$	1.86*(1.90)	7122.1	7112.7	0.054
$[Fe^{V}(N)(MePy_2tacn)](PF_6)_2$	1.64 (1.60)	7123.8	7113.9	0.57
[a][$Fe^{III}(N_3)$(cyclam – ac)]$^+$	1.94[a]	7123.0[a]	7112.4[c]	0.098[c]
[a][$Fe^{V}(N)$(cyclam – ac)]$^+$	1.61 (1.60) [a]	7124.1[a]	7113.9[c]	0.34[c]
[b][$Fe^{VI}(N)(Me_3$cyclam – ac)]$^{2+}$	1.57 (1.53)[b]	7125.0[b]	7114.4[c]	0.44[c]

*Values from X – ray diffraction. [a]Data from reference [44]. [b]Data from reference [33]. [c]Data from reference[45]

Theoretical Calculations.

The electronic structure of **1** and **2** was further explored with density functional theory (see details in Supporting Information). Compound **1** was modelled as a spin 1/2 Fe^{III} center as determined from experiment. The resulting geometry optimized structure predicts a short Fe^{III}-N bond of 1.90 Å and an $Fe^{III}N$-N_2 distance of 1.22 Å. These values correlate well with the crystallographically determined distances of 1.86 Å and 1.25 Å, respectively. In the case of **2**, a low-spin S = 1/2 Fe(V) centre is found to better match experimental data having a calculated Fe – nitride bond of 1.60 Å, matching the experimentally determined distance of 1.64 Å. A high-spin S = 3/2 iron(V) center on the other hand is predicted to have a bond length of 1.76 Å well outside the resolution limit of the EXAFS data (0.1 Å). Furthermore the XAS pre – edges for the series

were also calculated and found to correlate well to experiment (Supporting Figures S11 and S12). Difference density maps for the transitions highlight that for **2** the intense feature at 7114.2 eV arises from excitations to the d_z2 set of orbitals which have a σ* antibonding interaction with the nitride p_z orbital (Supporting Figure S12). As this is a σ – type interaction p – d mixing is more favoured (~2.7% p – character) than for transitions to π* (1.5% p – character) orbitals or transitions to non – bonding orbitals (~0.5% p – character) the latter forming the shoulder observed at 7112.4 eV.[43] Therefore an orbital picture emerges for **2** consistent with a low-spin Fe(V) centre. Using the notation $\Gamma(X)^n$ where Γ is the bonding nature, X is the predominant character of the orbital, and n its occupation number,[46] **2** is best described as having a $\delta(Fed_{xy})^2\pi^*(Fed_{xz,yz})^1\sigma^*(Fed_x2\text{-}y2)^0\sigma^*(Fed_z2)^0$ electronic arrangement (Figure 6). Such an electronic arrangement matches expectations from EPR and Mössbauer data which predict a high-valent spin 1/2 Fe center with significant orbital degeneracy as can be deduced from the drastic g-shifts of 1.55, 1.33 and 0.9. Furthermore the singly occupied π* $Fed_{xz/yz}$ shows a strong covalent Fe – N interaction having a ~30% Fe – character with 60% - N character similar to other highly covalent $[FeX]^{+n}$ cores (X = N, O) with the Fe – N bond order best described as 2.5.[44,47] Indeed, the strong Fe-N π interaction destabilizes the $d_{xz/yz}$ orbitals relative to the d_{xy} orbitals favouring the $(d_{xy})^2(d_{xz/yz})^1$ configuration.[44] Lastly, in **1** it is apparent that the occupied Fe 3d orbitals interact primarily with non-bonding orbitals with respect to the N_3 moiety (Figure 5). This further supports the premise that the $Fe^{III}N\text{-}N_2$ bond is activated by the strongly electrophilic character of the iron center surrounded by the neutral ligand framework which stabilizes the Fe – $^{-}$N–$^{+}$N ≡N resonance over the Fe – N=$^{+}$N=N^{-} resonance as previously postulated.[48]

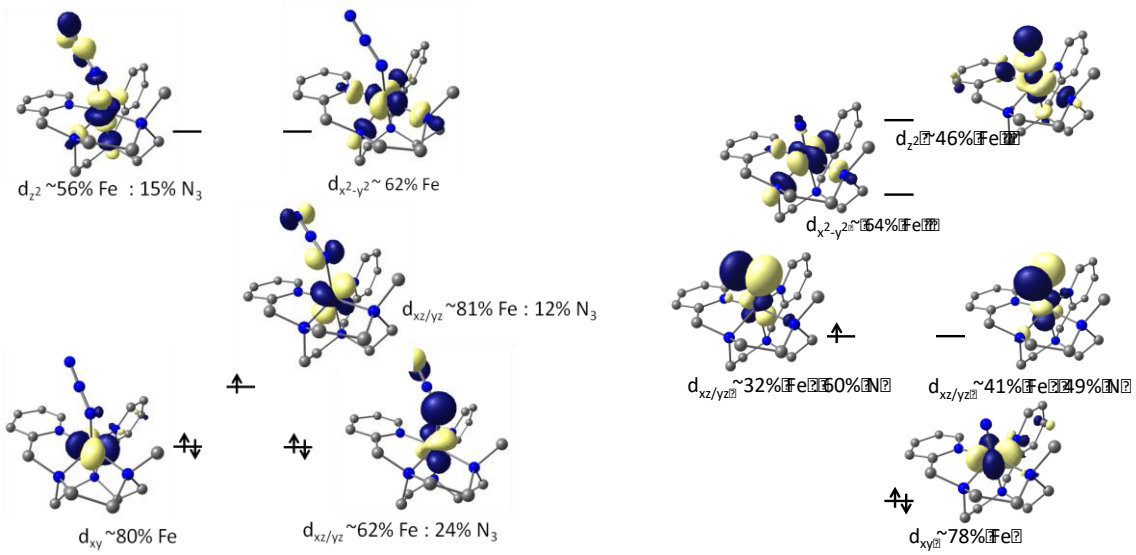

Figure 5. Schematic molecular orbital picture highlighting the d manifold of compounds **1** (left) and **2** (right), using quasi-restricted molecular orbitals at an isovalue of 0.06 (TPSSh/def2-TZVP//TPSS/def2-TZVP).[46]

Analysis of the formation and decay of 2 by gas evolution.

A mass spectrometry online system (EI – MS) was used to analyse the gas evolution during formation and decay of **2**. First, a frozen solution of **1 – ^{15}N** was analysed during photolysis. It was reasoned that this procedure should result in the production of N_2 gas, and that the use of isotopically labelled azide ligands may provide information about the mechanism (Figure 6). The photolysis of **1** was performed on a 4 mM acetone solution (1 ml) under Ar at 77 K using a 530 nm LED. The solution turned from purple to orange during the irradiation process. Despite of the change in colour, no N_2 evolution could be detected while being irradiated, presumably because the gas remains trapped inside the frozen solution. So, the analysis of the N_2 formed was performed by very slowly melting the sample (for 3 h) after 3.5 h of photolysis.

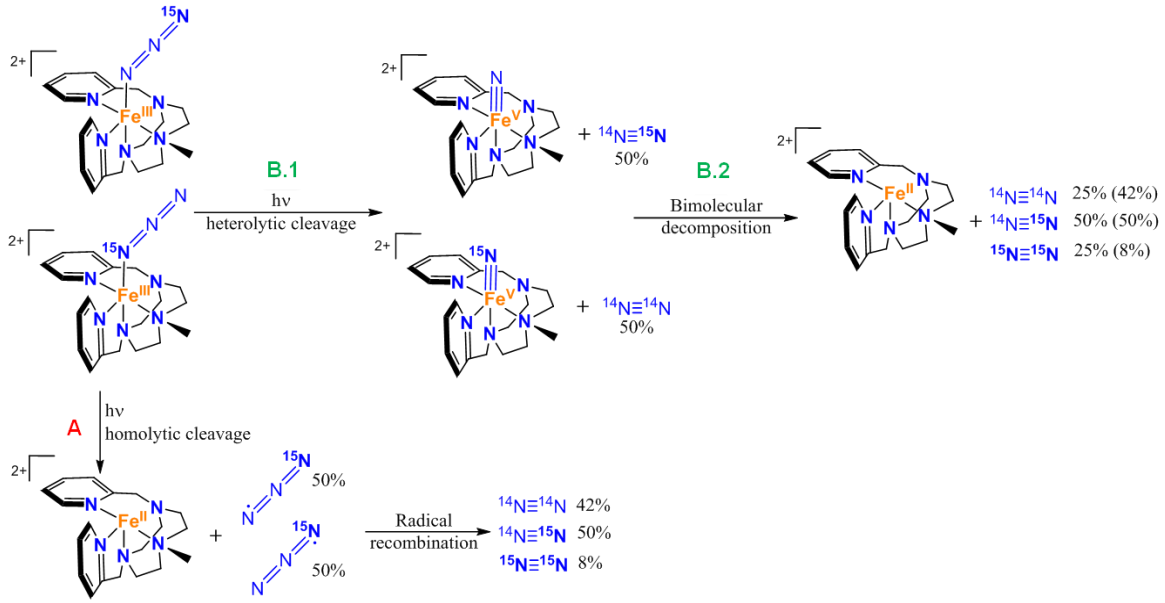

Figure 6. Reactivity of **1** upon irradiation, percentages are the N_2 amounts generated after photolysis (percentage in parentheses are the combination of B.1 and B.2).

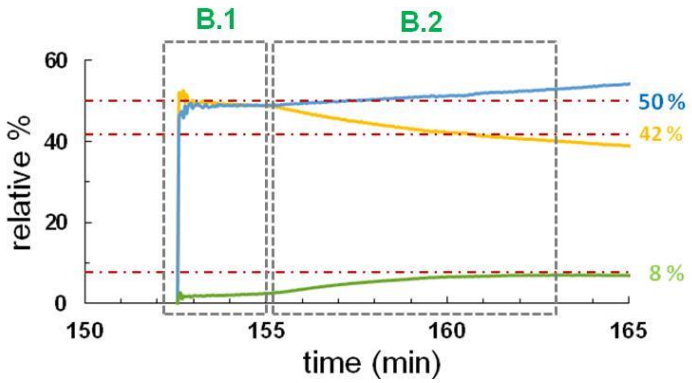

Figure 7: Evolution of the relative composition of the nitrogen gas isotopes (^{14}N – ^{14}N yellow line, ^{14}N – ^{15}N blue line and ^{15}N – ^{15}N green line) green line at the headspace of a solution of complex **2**, generated by irradiation of a solution of **1** (4 mM) in acetone at 530 nm LED for 3.5 hours under Ar at 77 K while slowly melting.

After slowly melting the sample for 2.5 h post-irradiation, N_2 release was observed. Importantly only $^{14}N^{14}N$ and $^{14}N^{15}N$ were detected, and more significantly, showing a ratio 1:1 which was maintained for a short period of time (*ca.* 5 min.). The ratio of 1:1 and the total absence of $^{15}N^{15}N$ clearly reflects the occurrence of step B.1 (Figures 6 and 7), the photooxidation of the iron (III) (**1**) to form the iron (V) species (**2**). Following this initial phase, that lasts for 5 minutes, the $^{14}N^{14}N$:$^{14}N^{15}N$ ratio starts to differ from 1:1, in favour of the latter. Moreover, at the same time $^{15}N^{15}N$ was detected. This change suggests a bimolecular decomposition of **2** (step B.2). For a short period of 6 - 8 minutes the proportion between $^{14}N^{14}N$:$^{14}N^{15}N$:$^{15}N^{15}N$ gases stayed close to the theoretical ratio of 42:50:8 (Figure 7). This ratio is the one expected for a scenario where the gas that emerges from the heterolytic cleavage of the N – N bond in **1** and the bimolecular decomposition of **2** are combined. Of interest, Krahe, Bill, and Neese[36] recently studied the decomposition of $[Fe^{III}(N_3)(\text{cyclam-ac})]^+$ and $[Fe^{III}(N_3)_2(\text{cyclam})]^+$. The study of the gases released after photolysis and subsequently decomposition was performed by ESI – MS and revealed ratios of $^{14}N^{14}N$:$^{14}N^{15}N$:$^{15}N^{15}N$ of ≈ 74:22:4 and ≈ 82:15:3, respectively. Those amounts of $^{14}N^{15}N$ and $^{15}N^{15}N$ are lower than the expected (42:50:8), most likely due to atmospheric N_2 contamination. Despite of that, the study provides clear evidence of the extrusion of $^{15}N^{15}N$ from a bimolecular decay pathway contributing to N_2 evolution, as the only source for the decomposition pathway of $Fe^V(N)$ species.[36] The fact that, in our reaction, the ratios do not remain constant over time suggests that the iron (V) species is not only decomposing through a bimolecular pathway, but additional non-identified paths must also be occurring. This is not surprising if we consider that **2** is expected to be a very electrophilic and reactive species, most likely capable of reacting with solvent or the ligand. Alternative decomposition pathways are also suggested by the detection of ions attributable to the CN^- moiety (mass of 26 and 27), which appear simultaneously with $^{15}N^{15}N$ gas release, presumably as **2** acquires some mobility upon the melting of the frozen solution. When the blue LED photolysed sample reported in Figure 3 showing a 25% low-spin Fe(II) and 75% S = 1/2 Fe(V) content, was left to warm up to room temperature under anaerobic conditions, a mixture of iron (II) and iron (III) was obtained (Figure S13 top). Most of the final mixture (~72%) consisted of a low-spin iron(III) center (isomer shift $\delta = 0.30$ mm·s^{-1}, quadrupole splitting $\Delta E_Q = 1.41$ mm·s^{-1}). Two distinct iron (II) components were also detected, the first of which was found to be in a high-spin state (21%), and the second (7%) in a low-spin state (isomer shift $\delta = 1.29$ and 0.57 mm·s^{-1}, quadrupole splitting $\Delta E_Q = 2.33$ and 0.77 mm·s^{-1} respectively). This again suggests that the decay of **2** involves multiple paths, instead of a clean decay of $[Fe^V(N)(\text{cyclam-ac})]^+$ to iron (II) upon N_2 generation, as previously observed by some of us.[36]

Finally, after monitoring of gases, HR – MS was performed in melted solution samples (Figure S13 bottom), confirming the conclusions of the Mössbauer analysis. The decomposition

mixture was composed mainly of $[Fe^{III}(OH)(MePy_2tacn)]^{2+}$ (m/z = 199.08) and a small amount of unreacted **1**. A small peak corresponding to the Fe^{V} species was also observed, presumably resulting from the cleavage of the residual **1.**

Gas phase reactivity

As **2** is not stable in solution its reactivity with organic molecules was studied in the gas phase. As shown above, the nitride dication $[Fe^{V}(N)(MePy_2tacn)]^{2+}$ can be prepared by gas – phase fragmentation of the corresponding azide dication $[Fe^{III}(N_3)(MePy_2tacn)]^{2+}$ (Figure S4 and S14). The fragmentation can also be achieved during electrospray ionization by setting harder ion – transfer conditions.[38] The generated nitride $[Fe^{V}(N)(MePy_2tacn)]^{2+}$ (m/z = 197.5) was mass – selected and subjected to reactions with different reagent gases.[49] Firstly, reactions with dimethyl sulfide and *cis* – cyclooctene were tested. As expected, the reactions proceed rapidly and the exclusive channel is a simple addition to either the sulfur atom of dimethyl sulfide or to the isolated double bond of *cis* – cyclooctene (Table 3, note that control experiments with the $[Fe^{III}(N_3)(MePy_2tacn)]^{2+}$ and $[Fe^{III}(OH)(MePy_2tacn)]^{2+}$ ions showed no comparable reactivity, Figure S16).

Next, we explored the reactivity of the nitride with 1, 3 – and 1, 4 – cyclohexadiene (Figure 8). The reactions are again dominated by addition of the alkene to the dication, but additional minor channels are observed as well. In the case of 1, 4 – cyclohexadiene, there is also a significant amount of the H_2 transfer which most probably corresponds to the formation of benzene. The same reaction with labelled 1, 4 – cyclohexadiene – 1, 2, 3, 4, 5, 6 – d_6 leads to the transfer of H_2, HD, and D_2 in a roughly 5:5:1 ratio. This suggests that the aromatization reaction proceeds in two steps: one of the two has a kinetic isotope effect (KIE) of ~ 3.6, whereas the other has a very small or negligible kinetic isotope effect (~ 1.4). The analysis does not permit to establish what is the relative order of the two steps. Interestingly, the ratio between the addition reaction and the H_2 transfer products is the same irrespective of the use of unlabeled cyclohexadiene or cyclohexadiene – 1, 2, 3, 4, 5, 6 – d_6 as substrate (78:22). This indicates that the step with the kinetic isotope effect is not kinetically competing with the N-transfer step. Similar reactivity is observed with 1,3 – cyclohexadiene except the aromatization reaction is much less abundant compared to the simple addition reaction.[25] These results are in agreement with previous reports from Schlangen *et al.* who also observed addition and H_2 transfer reactions with 1,3 – and 1,4 – cyclohexadienes.[31] In addition, Schlangen et al. observed NH_2 transfer, which was enabled by their ligand bearing amino groups in the vicinity of the nitride nitrogen (see below).

It is also interesting to compare the gas phase reactivity of **2** against cyclohexadienes with that exhibited by oxoiron(IV) complexes with tetra and pentadentate tacn based ligands.[50,51]

Reaction of the latter complexes with 1,4-cyclohexadiene entails a rate determining hydrogen atom transfer, followed by a reaction of the cyclohexadienyl radical with a second molecule of oxoiron(IV), to form benzene. In these reactions, the oxo-iron(IV) moiety acts as a single electron oxidant. In the gas phase, all iron(IV) – oxo complexes investigated so far react with 1,4-cyclohexadiene by hydrogen transfer as well. We could observe oxygen-transfer reactions of monocationic iron(IV)-oxo complexes with 1,4-cyclohexadiene, but it stayed a minor channel (5 – 20 %). Dicationic iron(IV) – oxo complexes did not yield oxygen-transfer products; neither addition products.[49,52] In solution, oxygen atom transfer towards the olefinic site does not take place, and is only observed when sulfides, which are particularly good oxygen atom acceptors, are used as substrates. When compared with the reactivity exhibited by **2**, these reactions suggest an enhanced competence of the iron(V) – nitride unit to engage in two e- oxidation processes.

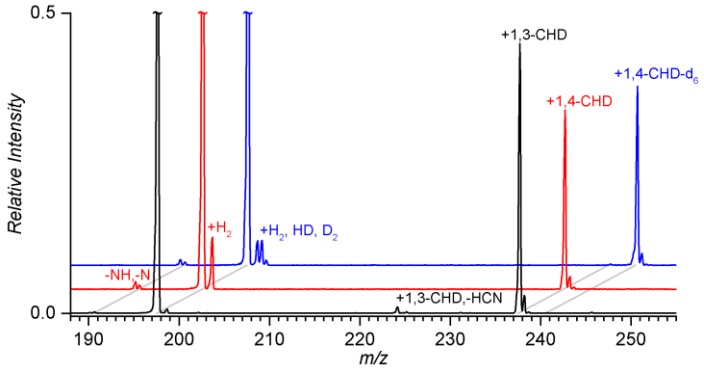

Figure 8. Reaction of $[Fe^{V}(N)(MePy_2tacn)]^{2+}$ (m/z = 197.5) with ~ 0.1 mTorr pressure of 1, 3 – cyclohexadiene (black trace), 1, 4 – cyclohexadiene (red trace) and 1, 4 – cyclohexadiene-1, 2, 3, 4, 5, 6 – d_6 (blue trace) at nominally zero collision energy. The assignments were corroborated by experiments with ^{15}N labelled nitride (Figure S17).

Table 3. Relative reaction rates[a] (k_{rel}) of $[Fe^{V}(N)(MePy_2tacn)]^{2+}$ dication with neutral molecules.

Reagent gas (R)	k_{rel}	Products (branching ratio)
1, 4 – cyclohexadiene	1.0	$[M+R]^{2+}$ (78), $[M+H_2]^{2+}$ (22)
1,4 – cyclohexadiene-d_6	1.0	$[M+R]^{2+}$ (78) , $[M+H_2]^{2+}$ (10), $[M+HD]^{2+}$ (10), $[M+D_2]^{2+}$ (2)
1,3 – cyclohexadiene	1.1	$[M+R]^{2+}$ (98), $[M+H_2]^{2+}$ (1) $[M+R-HCN]^{2+}$ (1)
cis – cyclooctene	1.5	$[M+R]^{2+}$ (100)
dimethyl sulfide	2.0	$[M+R]^{2+}$ (100)

[a] Relative to 1,4 – cyclohexadiene. Acetylene has also been tested, but no reaction was observed.

On the other hand, the exact nature of the formal H_2 transfer reaction cannot be ascertained at present. By analogy to the chemistry exhibited by oxo-iron(IV) complexes[49,51,53-55] it may be tentatively proposed to entail an initial hydrogen atom transfer, to form a

cyclohexadienyl radical and a $[Fe^{IV}(NH)(MePy_2tacn)]^{2+}$ species (pathway A in Scheme 2). In the current case, the latter species are not detected and therefore this step must be followed by a second and fast transfer of a hydrogen atom, to form benzene and $[Fe^{III}(NH_2)(MePy_2tacn)]^{2+}$ ($[M+H_2]^{2+}$). Alternatively, H_2 elimination can proceed via the aziridine intermediate (pathway B in Scheme 2). The low – spin nitride most probably initially adds to one of the double bonds of cyclohexadienes to form the aziridine ring. In the subsequent step, a hydrogen atom from the hydrocarbon migrates to the nitrogen atom. The second hydrogen transfer completes the reaction. This mechanism (in agreement with the experimental results) implies that the H_2 elimination from 1,3 – cyclohexadiene should be less abundant than for 1,4 – cyclohexadiene, because it has to be associated with hydrogen – ring walk (unlike for 1,4 – cyclohexadiene). It also explains the difference between our results and the results published previously by Schlangen *et al*.[31] Their ligand bears amino – groups in vicinity of the nitride nitrogen. The hydrogen transfer from the hydrocarbon at the stage of the aziridine intermediate is thus in competition with the hydrogen transfer from the ligand. We can see this process as well, but in very low abundance as trace NH elimination (see Figure 8). Furthermore, mechanism B can probably better account for the lack of an effect from deuteration on the ratio between the addition and H_2 transfer products. Nevertheless, validation of the elemental steps of this reaction will require extensive computational analysis, but the complexity of the problem, requiring the calculation of the different mechanisms for multiple spin states makes this task beyond the objectives of this work.[52]

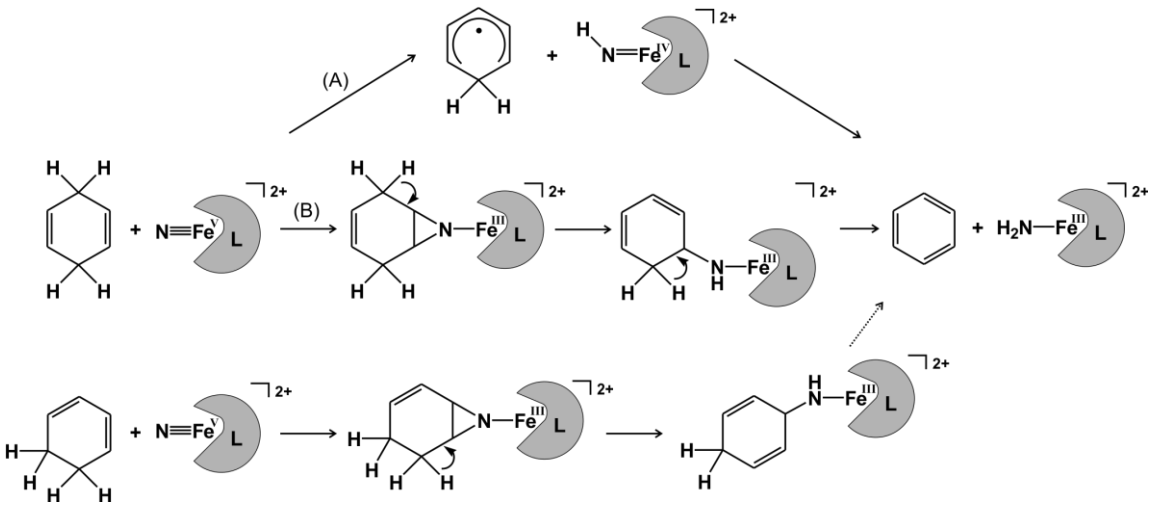

Scheme 2. Possible pathways in reaction of iron(V) – nitride with 1,3- and 1,4-cyclohexadiene.

Conclusions

Octahedral iron – azide complex **1** bearing a neutral pentadentate aminopyridine ligand based on the macrocycle triazacyclononane framework has been synthesised and studied as a potential precursor of high-valent iron – nitride species. Photolysis of **1** results in photooxidative cleavage of the N – N bond on the azide moiety, extruding N_2 to generate the high – valent iron (V) – nitride species **2** in the gas phase and also upon photolysis in frozen solution or as a powder at 77 K. Analysis of the N_2 gas mixtures generated upon photolysis of **1** by MS - online techniques give further evidence of an heterolytic N_2 extrusion. Iron(V) nitride species **2**, generated by photolysis of **1** was studied in detail by Mössbauer spectroscopy, EPR, SQUID and XAS, and identified as a low-spin (S = 1/2) iron(V) – nitrido species. XAS analysis confirmed the existence of a very short Fe – N bond in high concordance with previously reported high – valent iron (V) species. These species are highly reactive and rapidly decompose upon warming, so its reactivity in solution could not be investigated. MS – online techniques provide evidence that decomposition of **2** involves N – N bond formation. Reactivity of **2** in the gas phase indicates that the complex adds to olefinic sites. Reactions with cyclohexadienes also result in a formal H_2 transfer from the substrate to the $Fe^{V}(N)$ center, forming $Fe^{III}(NH_2)$ species and aromatization of the substrate. Compound **2** can also react with sulphides via a nucleophilic attack to the nitride moiety. Overall, the reactivity of the iron(V) – nitride species in the gas phase indicates that it is a competent $2e^-$ oxidant, showing reactivity not attained by iron(IV) species. In a more general context, the structural and chemical versatility of the aminopyridine ligand scaffold employed in this work is envisioned as a promising tool for further development of the chemistry of Fe(V) species.

Supporting Information

CIF file of complex **1**. Experimental details on the preparation of **1** and **3**, and of the generation of **2**. Spectroscopic data for the spectroscopic characterization of **1** and **2**. Spectroscopic and magnetic susceptibility data corresponding to the characterization of solid samples of **2**. UV-Vis spectra of the photolysis of **1** in solution. Spectra corresponding to gas phase reactivity of **2**. XYZ files of geometry optimized structures.

Acknowledgements

We acknowledge financial support from European Research Council (ERC-2009-StG-239910 to MC and ERC CoG No. 682275 to JR), MINECO of Spain and Fondo Europeo de Desarrollo Regional (CTQ2015-70795-P/BQU), and the Catalan DIUE of the Generalitat de Catalunya (2009SGR637). M.C. thank ICREA-Academia award. The project was supported by the Czech Science Foundation (14-20077S), and the COST action ECOSTBio. We thank Diamond Light Source for access to beamline B18 (proposal SP13863-1) that contributed to the results presented here. Also, we would like to thank SOLEIL for access to the SAMBA

beamline (proposal 20151019) as well as Dr. Landrot Gautier for his help with experimental setup.

References

(1) McDonald, A. R.; Que Jr., L. *Coord. Chem. Rev.* **2013**, *257*, 414.

(2) Groves, J. T. *J. Inorg. Biochem.* **2006**, *100*, 434.

(3) Costas, M.; Mehn, M. P.; Jensen, M. P.; Que Jr., L *Chem. Rev.* **2004**, *104*, 939.

(4) Hohenberger, J.; Ray, K.; Meyer, K. *Nat Commun* **2012**, *3*, 720.

(5) Wallar, B. J.; Lipscomb, J. D. *Chem. Rev.* **1996**, *96*, 2625.

(6) Nam, W.; Lee, Y.-M.; Fukuzumi, S. *Acc. Chem. Res.* **2014**, *47*, 1146.

(7) Sahu, S.; Goldberg, D. P. *J. Am. Chem. Soc.* **2016**, *138*, 11410.

(8) Rittle, J.; Green, M. T. *Science* **2010**, *330*, 933.

(9) Krebs, C.; Galonić Fujimori, D.; Walsh, C. T.; Bollinger, J. M. *Acc. Chem. Res.* **2007**, *40*, 484.

(10) Banerjee, R.; Proshlyakov, Y.; Lipscomb, J. D.; Proshlyakov, D. A. *Nature* **2015**, *518*, 431.

(11) Zandi, O.; Hamann, T. W. *Nat Chem* **2016**, *8*, 778.

(12) Codola, Z.; Gomez, L.; Kleespies, S. T.; Que, L., Jr.; Costas, M.; Lloret-Fillol, J. *Nat Commun* **2015**, *6*.

(13) Panda, C.; Debgupta, J.; Diaz Diaz, D.; Singh, K. K.; Gupta, S. S.; Dhar, B. B. *J. Am. Chem. Soc.* **2014**, *136*, 12273.

(14) Hoffman, B. M.; Lukoyanov, D.; Yang, Z.-Y.; Dean, D. R.; Seefeldt, L. C. *Chem. Rev.* **2014**, *114*, 4041.

(15) Mehn, M. P.; Peters, J. C. *J. Inorg. Biochem.* **2006**, *100*, 634.

(16) Smith, J. M.; Subedi, D. *Dalton Trans.* **2012**, *41*, 1423.

(17) Berry, J. F. *Comm. Inorg. Chem.* **2009**, *30*, 28.

(18) Smith, J. M. In *Prog. Inorg. Chem., Vol 58*; Karlin, K. D., Ed.; John Wiley & Sons Inc: Hoboken, 2014; Vol. 58, p 417.

(19) Wagner, W. D.; Nakamoto, K. *J. Am. Chem. Soc.* **1989**, *111*, 1590.

(20) Hendrich, M. P.; Gunderson, W.; Behan, R. K.; Green, M. T.; Mehn, M. P.; Betley, T. A.; Lu, C. C.; Peters, J. C. *Proc. Nat. Acad. Sci.* **2006**, *103*, 17107.

(21) Betley, T. A.; Peters, J. C. *J. Am. Chem. Soc.* **2004**, *126*, 6252.

(22) Vogel, C.; Heinemann, F. W.; Sutter, J.; Anthon, C.; Meyer, K. *Angew. Chem. Int. Ed.* **2008**, *47*, 2681.

(23) Scepaniak, J. J.; Fulton, M. D.; Bontchev, R. P.; Duesler, E. N.; Kirk, M. L.; Smith, J. M. *J. Am. Chem. Soc.* **2008**, *130*, 10515.

(24) Scepaniak, J. J.; Bontchev, R. P.; Johnson, D. L.; Smith, J. M. *Angew. Chem. Int. Ed.* **2011**, *50*, 6630.

(25) Lee, W.-T.; Juarez, R. A.; Scepaniak, J. J.; Muñoz, S. B.; Dickie, D. A.; Wang, H.; Smith, J. M. *Inorg. Chem.* **2014**, *53*, 8425.

(26) Muñoz, S. B.; Lee, W.-T.; Dickie, D. A.; Scepaniak, J. J.; Subedi, D.; Pink, M.; Johnson, M. D.; Smith, J. M. *Angew. Chem. Int. Ed.* **2015**, *54*, 10600.

(27) Scepaniak, J. J.; Margarit, C. G.; Harvey, J. N.; Smith, J. M. *Inorg. Chem.* **2011**, *50*, 9508.

(28) Scepaniak, J. J.; Young, J. A.; Bontchev, R. P.; Smith, J. M. *Angew. Chem. Int. Ed.* **2009**, *48*, 3158.

(29) Grapperhaus, C. A.; Mienert, B.; Bill, E.; Weyhermüller, T.; Wieghardt, K. *Inorg. Chem.* **2000**, *39*, 5306.

(30) Meyer, K.; Bill, E.; Mienert, B.; Weyhermüller, T.; Wieghardt, K. *J. Am. Chem. Soc.* **1999**, *121*, 4859.

(31) Schlangen, M.; Neugebauer, J.; Reiher, M.; Schröder, D.; López, J. P.; Haryono, M.; Heinemann, F. W.; Grohmann, A.; Schwarz, H. *J. Am. Chem. Soc.* **2008**, *130*, 4285.

(32) Scepaniak, J. J.; Vogel, C. S.; Khusniyarov, M. M.; Heinemann, F. W.; Meyer, K.; Smith, J. M. *Science* **2011**, *331*, 1049.

(33) Berry, J. F.; Bill, E.; Bothe, E.; George, S. D.; Mienert, B.; Neese, F.; Wieghardt, K. *Science* **2006**, *312*, 1937.

(34) Song, Y.-F.; Berry, J. F.; Bill, E.; Bothe, E.; Weyhermüller, T.; Wieghardt, K. *Inorg. Chem.* **2007**, *46*, 2208.

(35) Cutsail Iii, G. E.; Stein, B. W.; Subedi, D.; Smith, J. M.; Kirk, M. L.; Hoffman, B. M. *J. Am. Chem. Soc.* **2014**, *136*, 12323.

(36) Krahe, O.; Bill, E.; Neese, F. *Angew. Chem. Int. Ed.* **2014**, *53*, 8727.

(37) Torres-Alacan, J.; Das, U.; Filippou, A. C.; Vöhringer, P. *Angew. Chem. Int. Ed.* **2013**, *52*, 12833.

(38) Schröder, D.; Schwarz, H.; Aliaga-Alcalde, N.; Neese, F. *Eur. J. Inorg. Chem.* **2007**, *2007*, 816.

(39) Nakamoto, K. *Infrared and Raman Spectra of Inorganic and Coordination Compounds. Part B: Application in Coordination, Organometallic, and Bioinorganic Chemistry, 5th Edition*; John Wiley & Sons, Inc.: Hoboken, New Jersey, 2009.

(40) Company, A.; Sabenya, G.; Gonzalez-Bejar, M.; Gomez, L.; Clemancey, M.; Blondin, G.; Jasniewski, A. J.; Puri, M.; Browne, W. R.; Latour, J. M.; Que Jr., L. ; Costas, M.; Perez-Prieto, J.; Lloret-Fillol, J. *J. Am. Chem. Soc.* **2014**, *136*, 4624.

(41) Aasa, R. V., T. *J. Mag. Res.* **1975**, *19*, 308.

(42) Krahe, O. M., Rheinischen Friedrich-Wilhelms-Universität Bonn, 2016.

(43) Westre, T. E.; Kennepohl, P.; DeWitt, J. G.; Hedman, B.; Hodgson, K. O.; Solomon, E. I. *J. Am. Chem. Soc.* **1997**, *119*, 6297.

(44) Aliaga-Alcalde, N.; DeBeer George, S.; Mienert, B.; Bill, E.; Wieghardt, K.; Neese, F. *Angew. Chem. Int. Ed.* **2005**, *44*, 2908.

(45) Chandrasekaran, P.; Stieber, S. C. E.; Collins, T. J.; Que Jr. L. ; Neese, F.; DeBeer, S. *Dalton Trans.* **2011**, *40*, 11070.

(46) Ye, S.; Geng, C.-Y.; Shaik, S.; Neese, F. *Phys. Chem. Chem. Phys.* **2013**, *15*, 8017.

(47) Berry, J. F.; DeBeer George, S.; Neese, F. *Chem. Chem. Phys.* **2008**, *10*, 4361.

(48) Dori, Z.; Ziolo, R. F. *Chem. Rev.* **1973**, *73*, 247.

(49) Andris, E.; Jasik, J.; Gomez, L.; Costas, M.; Roithova, J. *Angew. Chem. Int. Ed.* **2016**, *55*, 3637.

(50) Company, A.; Prat, I.; Frisch, J. R.; Ballesté, R. M.; Güell, M.; Juhász, G.; Ribas, X.; Münck, E.; Luis, J. M.; Que Jr., L.; Costas, M. *Chem. Eur. J.* **2011**, *17*, 1622.

(51) Wang, D.; Ray, K.; Collins, M. J.; Farquhar, E. R.; Frisch, J. R.; Gomez, L.; Jackson, T. A.; Kerscher, M.; Waleska, A.; Comba, P.; Costas, M.; Que Jr., L. *Chem. Sci.* **2013**, *4*, 282.

(52) Andris, E.; Navrátil, R.; Jašík, J.; Terencio, T.; Srnec, M.; Costas, M.; Roithová, J. *J. Am. Chem. Soc.* **2017**, *139*, 2757.

(53) Cho, K.-B.; Hirao, H.; Shaik, S.; Nam, W. *Chem. Soc. Rev.* **2016**, *45*, 1197.

(54) Cho, K.-B.; Wu, X.; Lee, Y.-M.; Kwon, Y. H.; Shaik, S.; Nam, W. *J. Am. Chem. Soc.* **2012**, *134*, 20222.

(55) Kaizer, J.; Klinker, E. J.; Oh, N. Y.; Rohde, J.-U.; Song, W. J.; Stubna, A.; Kim, J.; Munck, E.; Nam, W.; Que Jr., L. *J. Am. Chem. Soc.* **2004**, *126*, 472.

TOC

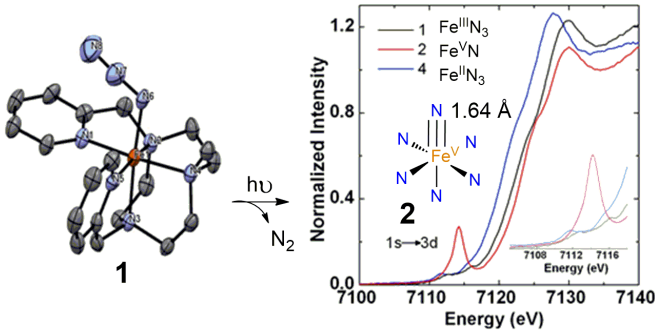

δ = -0.01 mm·s^{-1}, ΔEq = 1.02 mm·s^{-1}